Hindawi
Adsorption Science & Technology
Volume 2022, Article ID 2548390, 14 pages
https://doi.org/10.1155/2022/2548390

Research Article

Effect of Analytical Particle Size on Pore Structure of High Volatile Bituminous Coal and Anthracite Using Low-Pressure N_2 and CO_2 Adsorption

Zheng Dang,[1] Xiaoming Wang ,[1] Shihui Hou ,[2] and Sidong Pan[1]

[1]*Key Laboratory of Tectonics and Petroleum Resources, China University of Geosciences, Wuhan 430074, China*
[2]*Laboratory of Geotechnical Engineering, Jinggangshan University, Ji'an 343000, China*

Correspondence should be addressed to Xiaoming Wang; sunwxm@cug.edu.cn and Shihui Hou; houshihui@jgsu.edu.cn

Received 26 August 2022; Accepted 28 October 2022; Published 14 November 2022

Academic Editor: Anjani Ravi Kiran Gollakota

To investigate the effect of analytical particle size on pore structure, mesopore (2-50 nm) and micropore (<2 nm) characteristics of high volatile bituminous coal and anthracite with different particle size were determined using low-pressure N_2/CO_2 adsorption analyses. Mesopore structure parameters in the two coals increase with decreasing particle size, which are attributed to the opening of closed mesopores during the pulverization process. The closed mesopores with different pore size ranges are opened with a certain percentage in high volatile bituminous coal, but opened irregularly in anthracite during pulverization. Micropore structure parameters of the two coals show different variations with decreasing particle size, which are not related to the reconstituted micropore structure. Mineral matter contributes more mesopores than organic matter in anthracite and exerts the negative effect on micropore in the two coals. An evolution model is established to elaborately describe the change of pore structure during the pulverization process, where mineral matter plays a mediating role in the effect of particle size on pore structure.

1. Introduction

Coalbed methane (CBM), a kind of unconventional gas resources, has been commercially employed as the supplement of conventional gas resources in the last decades [1] and for the safe of coal mining [2]. Pore structure characteristics of coal, including pore diameter, pore volume, specific surface area (SSA), pore size distribution (PSD), pore shape and pore connectivity, are critical to CBM storage and transport during CBM exploitation [3–7]. Pores in coal are usually classified into three subtypes as micropores (pore diameter <2 nm), mesopores (pore diameter of 2–50 nm), and macropores (pore diameter > 50 nm), according to the International Union of Pure and Applied Chemistry (IUPAC) [8]. Quantitative pore structure of coal is important for coal utilization [9], CBM exploration [10], and gas outburst prevention [11].

Pore structure of coal is highly heterogeneous and influenced by coal rank [12, 13], maceral compositions [14], and mineral matter [15]. Among them, coal rank is considered to be the dominant factor. With increasing coal rank, pore volume first decreases and then increases [16] due to the change in coal molecular structure [17]. Pore complexity increases, while pore geometry, pore genetic type, and pore connectivity vary considerably with coal rank [18–20]. Pore structure depends on maceral compositions. Vitrinite is reported to contain fewer mesopores and more micropores than inertinite with the same coal rank, and liptinite contains larger macropores [14, 21]. Strong negative correlation has been documented between mineral matter and micropore, but the correlation of mineral matter with mesopore remains uncertain [15].

Different detective methods can reflect different pore structure characterization [9]. Multiple detective techniques are adopted to extensively investigate pore structure in coal, including small-angle neutron scattering (SANS) [22], scanning electron microscopy (SEM) [23], low-pressure gas (N_2, CO_2, and Ar) adsorption [24, 25], mercury injection capillary pressure (MICP) [26], nuclear magnetic resonance

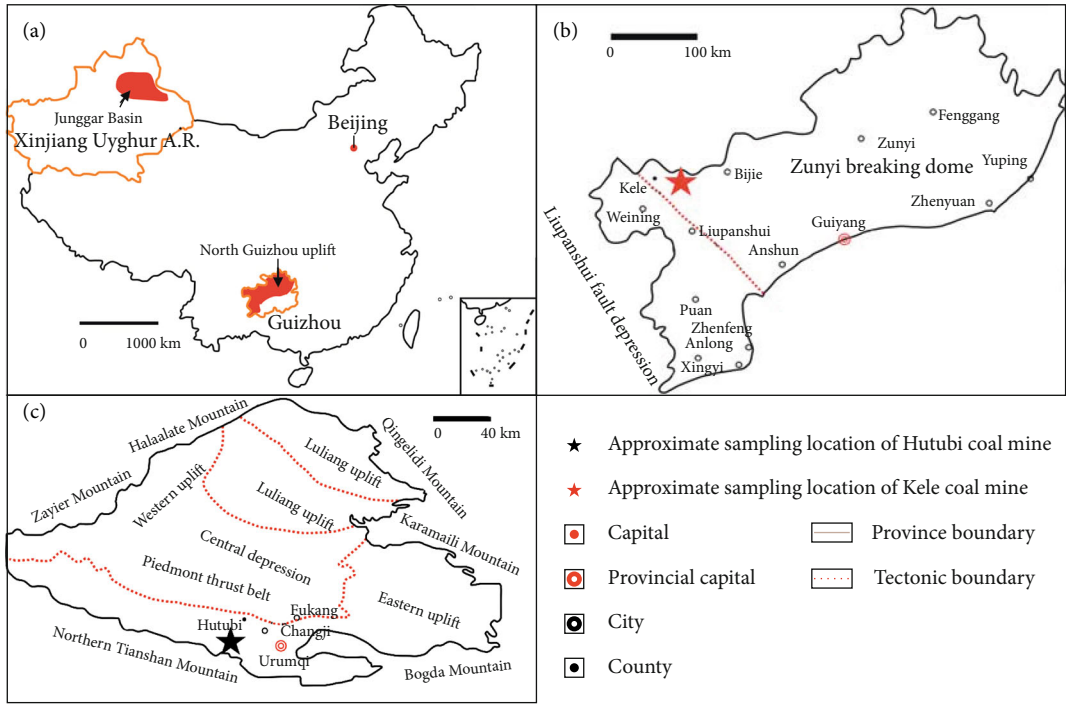

Figure 1: Positions of sampling locations in Kele coal mine (a, b) and Hutubi coal mine (a, c).

(NMR) [9], and X-ray computed tomography (CT) [27]. Compared with other methods, low-pressure N_2 and CO_2 adsorption can be more economical and convenient to characterize mesopores and micropores, respectively [24, 28], which have been extensively adopted to investigate pore structure in coal [29]. Due to the comprehensive influence of activated diffusion, pore shrinkage and coal swelling, micropores are inaccessible to N_2 molecules but accessible to CO_2 molecules [14, 30, 31], thus the probing pore diameters by CO_2 adsorption and N_2 adsorption are in the range of micropores and mesopores, respectively [32]. Coal samples are always crushed to a certain particle size for low-pressure N_2 and CO_2 adsorption. What is noteworthy is that, pore structure of coal can be damaged by pulverization [11]. Therefore, the influence of particle size on pore structure of coal needs to be analyzed.

Pore structure of coal changes with particle size [24, 32–34]. Mastalerz et al. [24] and Hou et al. [32] found that there is an increasing trend in mesopore SSA and volume with decreasing particle size. They attributed to the changes in pore structure and disequilibrium adsorption during crushing. Similar trend has been proved in anthracite by Si et al. [34] and Chen et al. [33], and they thought that the increasing mesopore SSA and volume are related to the opening of closed pores as a result of pulverization. The comparison in the experimental results between Wang et al. [35] and Hou et al. [32] showed that the change in mesopore structure parameters of low-rank coal is more significant than that of high-rank coal. Moreover, Mastalerz et al. [24] and Hou et al. [32] documented that micropore characteristics are independent of particle size, while Zhang et al. [36] demonstrated a positive correlation between micropore structure parameters and particle size. The effect of particle size on micropore structure is still uncertain. An evolution model of pore structure during the crushing process is needed to describe the effect of particle size on pore structure in detail.

The Junggar Basin and the Qianxi area are the main CBM blocks in China. Coal rank of the CBM target coal seams in the two blocks is quite different. Previous studies have proved that the CBM target coal seams in the two blocks have significantly different gas adsorption capacities [18, 37]. Two coal samples of high volatile bituminous coal and anthracite were collected from the two blocks. The pore structure of the two different rank coals with varying particle size was systematically characterized using low-pressure N_2/CO_2 adsorption for the following purposes: (1) to reveal the effect of particle size on pore structure, and (2) to establish a model of variation in pore structure during the crushing process. This research has a certain reference value for selecting the optimal particle size for low-pressure N_2/CO_2 adsorption, and provides the insights into the differences in adsorption capacity resulted from particle size effect.

2. Materials and Methods

2.1. Sample Collection and Pretreatment. High volatile bituminous coal was obtained from the Hutubi coal mine located in the Junggar Basin, Xinjiang Uyghur A. R., China (hereinafter Coal XJ). Anthracite was collected from the Kele coal mine located in the North Guizhou uplift, Guizhou Province, China (hereinafter Coal GZ). The location and stratigraphic column of the sampled coal mines are shown in Figures 1 and 2, respectively. Coal samples were crushed and then sieved into subsamples with the following five particle size fractions: 18–35 mesh (0.50–1.00 mm), 35–60 mesh

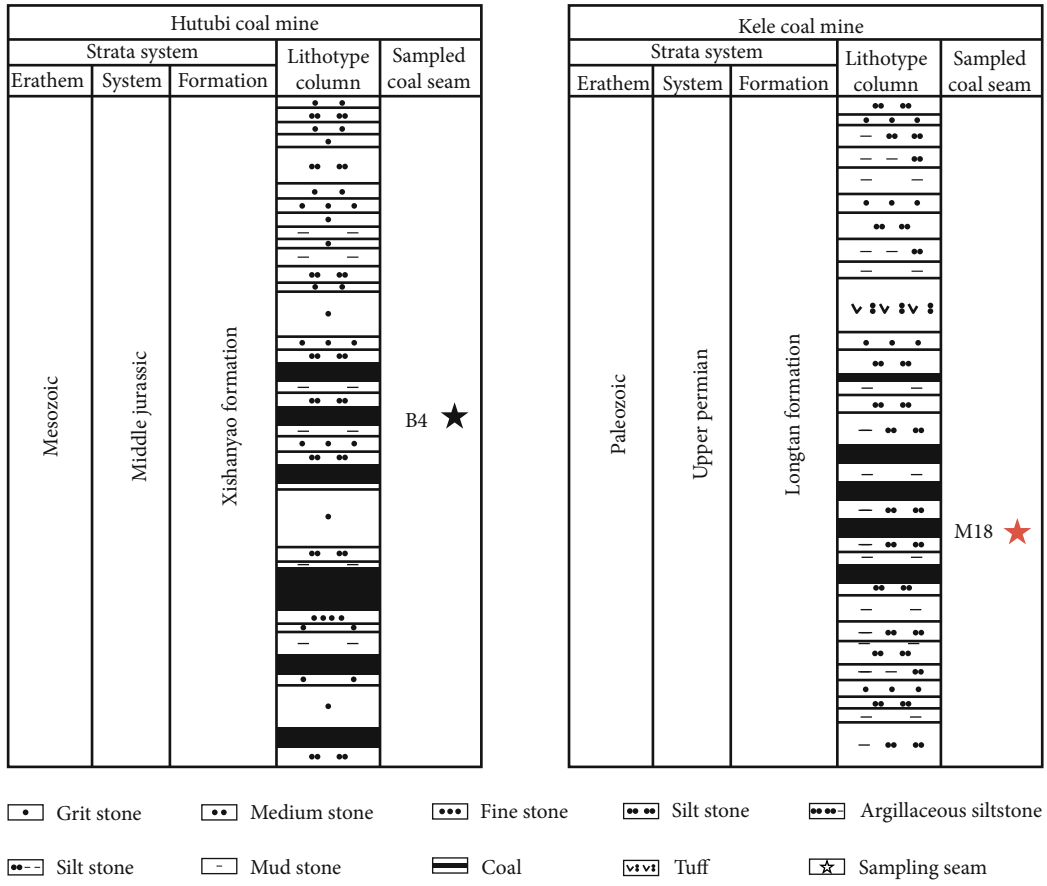

Figure 2: Stratigraphic columns and markers of sampling coal seams of the two coal mines.

Table 1: Basic characteristics of the coal samples with different particle sizes.

Sample	Particle size range, mm	Proximate analysis			Maceral composition			R_O, %	Coal rank
		M_{ad}, %	A_d, %	V_{daf}, %	V, %	I, %	V/I		
Coal XJ	0.50–1.00	2.74	22.04	28.93	73.00	27.00	2.7	0.883	High volatile bituminous coal
	0.25–0.50	2.46	13.46	26.02	59.92	40.08	1.5		
	0.125–0.250	2.55	12.59	26.85	55.40	44.60	1.2		
	0.063–0.125	2.43	11.78	26.68	51.04	48.96	1.1		
	0.032–0.063	2.36	15.54	24.96	44.49	55.51	0.8		
Coal GZ	0.50–1.00	3.86	8.42	5.64	93.00	7.00	13.3	2.622	Anthracite
	0.25–0.50	4.97	10.22	6.10	88.45	11.55	7.7		
	0.125–0.250	5.09	11.03	5.58	87.72	12.28	7.2		
	0.063–0.125	5.00	13.16	7.07	84.42	15.58	5.4		
	0.032–0.063	4.93	17.23	10.06	79.37	20.63	3.9		

R_o = mean vitrinite reflectance in oil immersion; M_{ad} = moisture content on air-dry basis; A_d = ash yield on dry basis; V_{daf} = volatile matter yield on dry and ash-free basis; V = vitrinite content; I = inertinite content; V/I = ratio of vitrinite content to inertinite content.

(0.25–0.50 mm), 60–120 mesh (0.125–0.250 mm), 120–230 mesh (0.063–0.125 mm), and 230–450 mesh (0.032–0.063 mm). Low-pressure N_2/CO_2 adsorption and coal quality analyses were conducted on every particle size fraction. Coal samples with particle size lower than 18 mesh (1 mm) were used for vitrinite reflectance measurement.

2.2. Coal Quality Analysis. The mean vitrinite reflectance (%, R_O) was measured following ASTM D2798-11a, and the coal samples were classified according to ASTM D388-19. Proximate analysis and maceral composition analysis were conducted on all subsamples according to ASTM D3172-13 and the 500-point grid method, respectively.

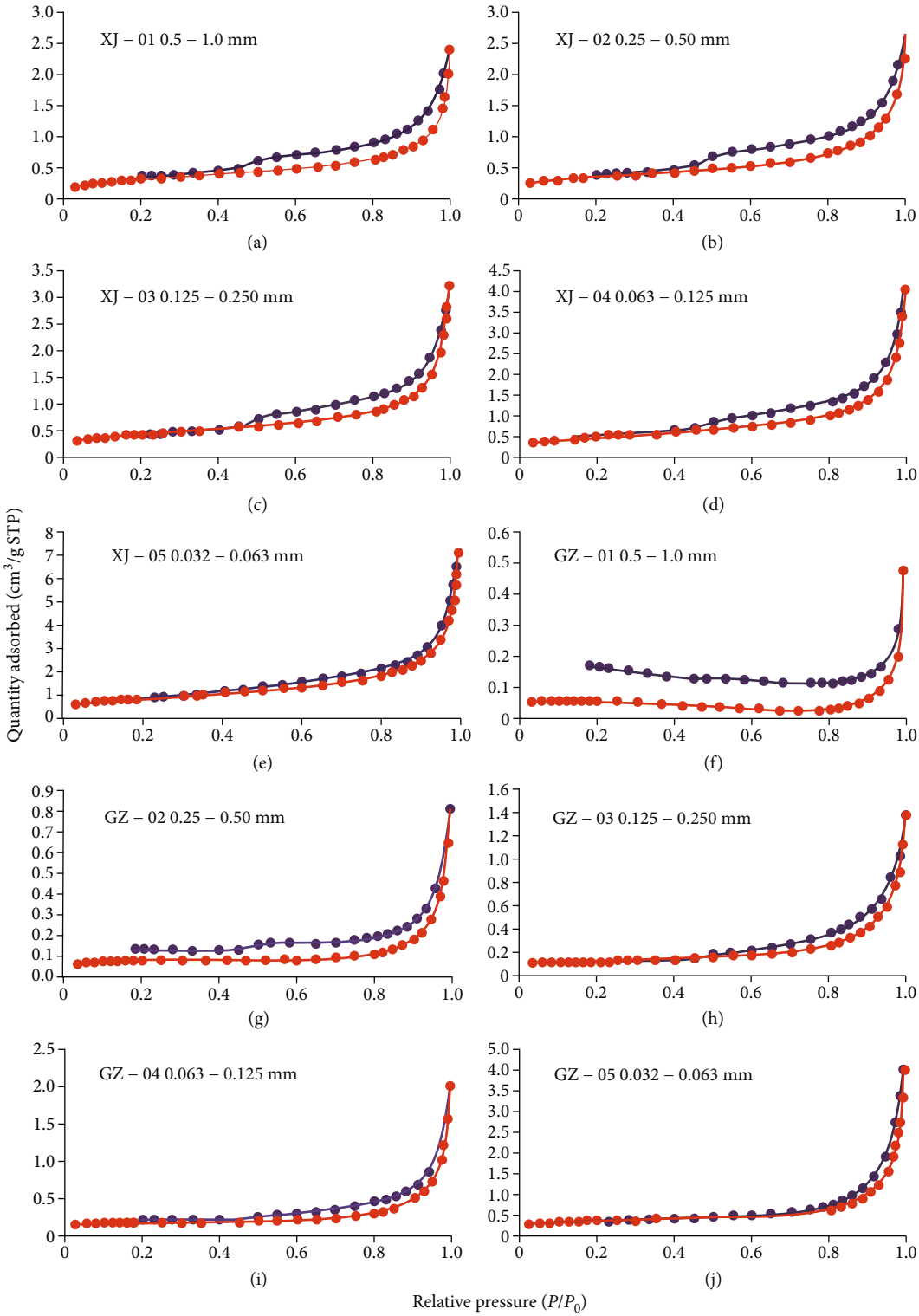

Figure 3: Low-pressure N_2 adsorption-desorption isotherms of the subsamples with different particle sizes: (a–e) Coal XJ; (f–j) Coal GZ.

2.3. Low-Pressure Gas Adsorption Analysis. Low-pressure gas adsorption experiment for all the subsamples was performed on Micromeritics ASAP 2020 using N_2 and CO_2 as adsorbates. Before gas adsorption, 2–3 g subsamples were dried and evacuated at 110°C for 900 mins to remove preadsorbed moisture and residual gas.

In N_2 adsorption, the subsamples were analyzed at the liquid N_2 temperature (77.35 K at 101.3 kPa) for collecting adsorption and desorption isotherms with relative pressure (P/P_0, where P is the actual gas pressure, and P_0, the vapor pressure of the adsorbing gas, is 774 mmHg (103.19 kPa) at 77.35 K) from 0 to 0.995. Equilibrium interval was set as 10 s,

Table 2: Pore structure parameters using low-pressure gas adsorption analysis on the coal subsamples with different particle sizes.

Subsample no.	Particle size range	N_2 adsorption		CO_2 adsorption	
		Mesopore SSA	Mesopore volume	Micropore SSA	Micropore volume
	mm	m^2/g	cm^3/g	m^2/g	cm^3/g
XJ-01	0.50–1.00	1.10	0.0036	117.1	0.0153
XJ-02	0.25–0.50	1.33	0.0040	127.5	0.0192
XJ-03	0.125–0.250	1.51	0.0050	122.6	0.0209
XJ-04	0.063–0.125	1.72	0.0062	124.6	0.0223
XJ-05	0.032–0.063	3.12	0.0109	117.2	0.0204
GZ-01	0.50–1.00	0.20	0.0007	257.3	0.0394
GZ-02	0.25–0.50	0.26	0.0012	241.5	0.0412
GZ-03	0.125–0.250	0.48	0.0021	216.2	0.0402
GZ-04	0.063–0.125	0.62	0.0030	197.5	0.0368
GZ-05	0.032–0.063	1.24	0.0060	172.7	0.0339

SSA: specific surface area.

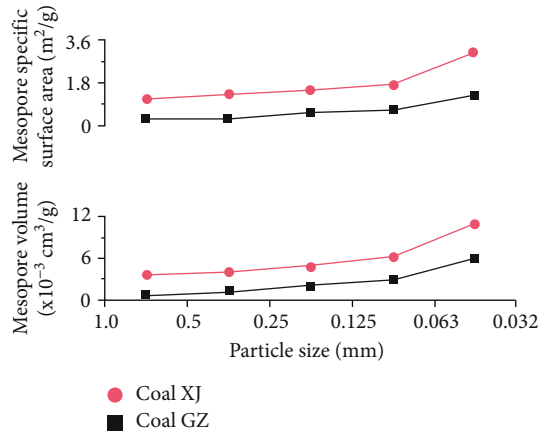

Figure 4: Variations in mesopore structure parameters of the coal samples with different particle sizes.

and absolute pressure tolerance and relative pressure tolerance were set as 5 mmHg (0.6666 kPa) and 5%, respectively. The adsorption branch was used to calculate mesopore SSA, volume, and PSD. The mesopore SSA is determined by Brunauer-Emmett-Teller (BET) theory, and the volume and PSD of mesopore were obtained by Barrett-Joyner-Halenda (BJH) theory. Repeatability of low-pressure N_2 adsorption analysis for the instrumentation is approximately 2%.

For CO_2 adsorption, only adsorption curve was obtained in the relative pressure (P/P_0) range between 4.8×10^{-4} and 3.1×10^{-2} at a temperature of 273 K with a mixture of ice and water. The P_0 of CO_2 is 2.6142×10^4 mmHg (3.485 MPa), and the corresponding absolute pressure varies from 10 mmHg (1.69 kPa) to 811 mmHg (108.12 kPa). During adsorption process, equilibrium interval was set as 30 s, and absolute pressure tolerance and relative pressure tolerance were set as 5 mmHg (0.6666 kPa) and 5%, respectively. Micropore volume and PSD were determined by density functional theory (DFT) method, and micropore SSA was calculated based on Dubinin-Astakhov (D-A) equation. Repeatability of low-pressure CO_2 adsorption analysis for the instrumentation is about 1%.

Pore structure parameters and PSDs were calculated and exported using the MicroActive software. The principles of assumption, interpretation, and significance for pore structure parameter calculation have been discussed in detail by Rouquerol et al. [38].

3. Results

3.1. Coal Characteristics. The coal basic characteristics, including proximate analysis and petrographic analysis (mineral-matter free), are listed in Table 1. The R_O values of Coal XJ and Coal GZ are 0.883% and 2.662%, indicating high-volatile bituminous coal and anthracite, respectively. Moisture contents are less than 6% and independent of particle size. The ash yields of the two coal samples show different trends with decreasing particle size. The ash yield of Coal XJ decreases from 22.04% to 11.78%, while that of Coal GZ increases from 8.42% to 17.23%.

Maceral composition is related to particle size. For Coal GZ, the dominant component vitrinite decreases from 93.00% to 79.37% during the crushing process, while inertinite increases from 7.00% to 20.63%. For Coal XJ, vitrinite

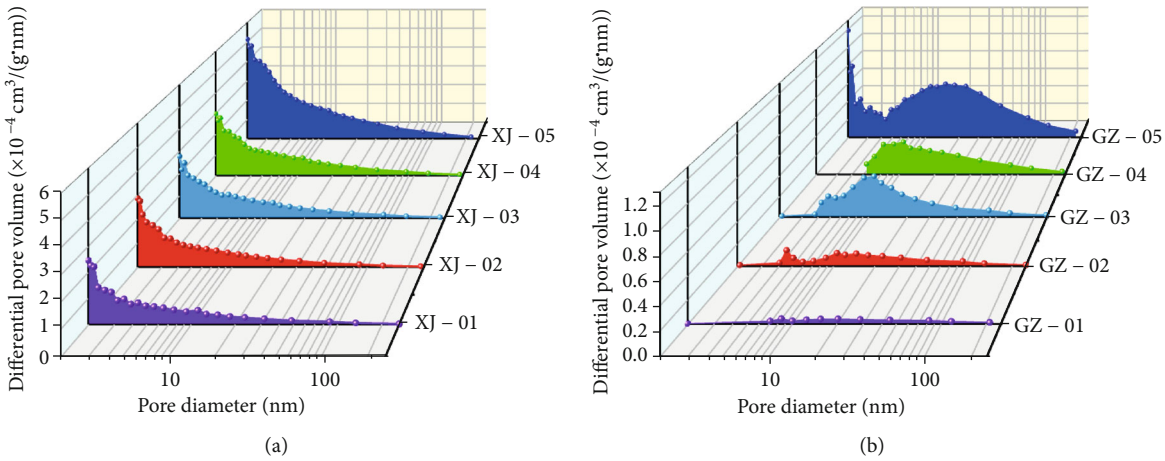

Figure 5: Pore size distributions of the coal subsamples with different particle sizes using low-pressure N_2 adsorption analysis. (a) Coal XJ (XJ-01 to XJ-05 represent Coal XJ with particle size from 0.5-1.0 mm to 0.032-0.063 mm). (b) Coal GZ (GZ-01 to GZ-05 represent Coal GZ with particle size from 0.5-1.0 mm to 0.032-0.063 mm).

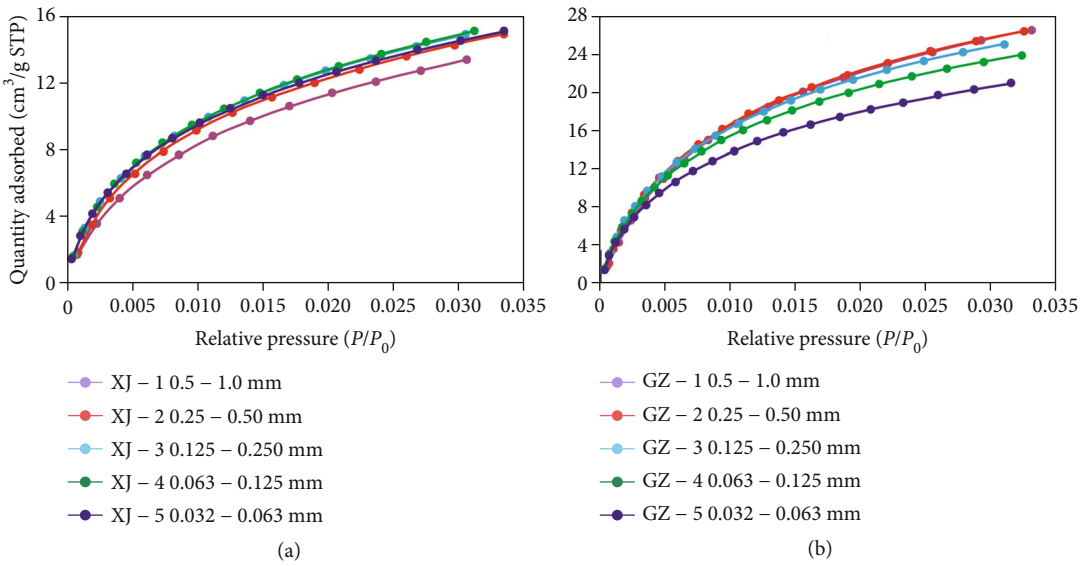

Figure 6: Low-pressure CO_2 adsorption isotherms of the coal subsamples with different particle sizes: (a) Coal XJ; (b) Coal GZ.

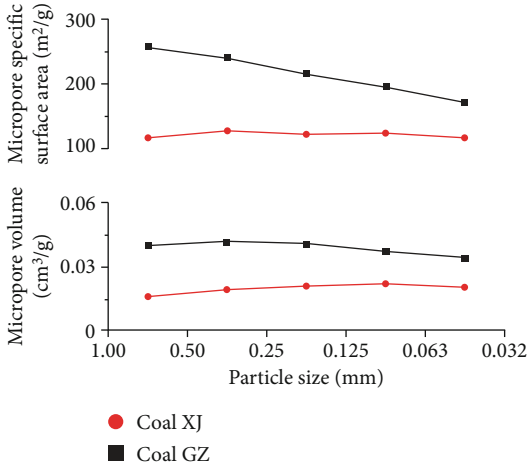

Figure 7: Variations in micropore structure parameters in the coal samples with different particle sizes.

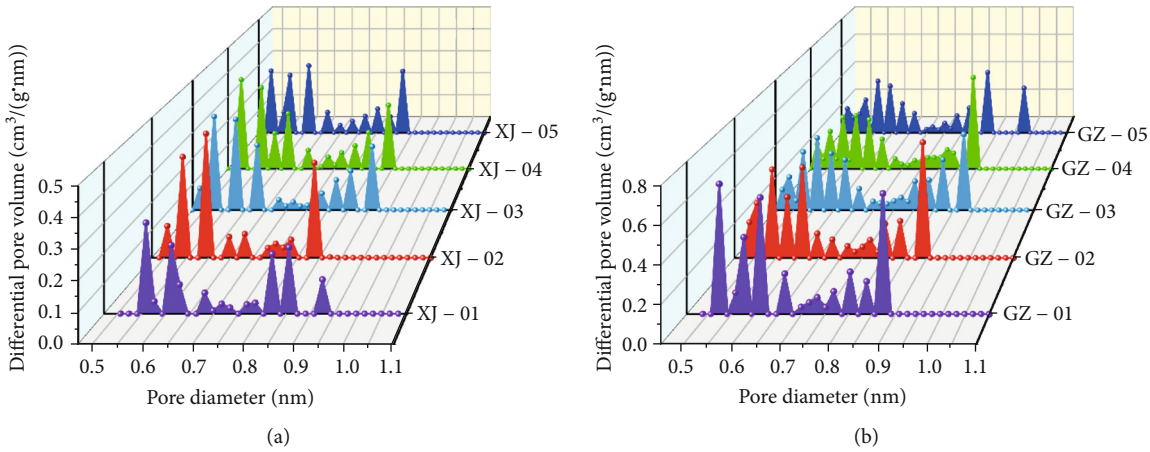

Figure 8: Pore size distributions of microp ores in the coal samples with different particle sizes. (a) Coal XJ (XJ-01 to XJ-05 represent Coal XJ with particle size from 0.5-1.0 mm to 0.032-0.063 mm). (b) Coal GZ (GZ-01 to GZ-05 represent Coal GZ with particle size from 0.5-1.0 mm to 0.032-0.063 mm).

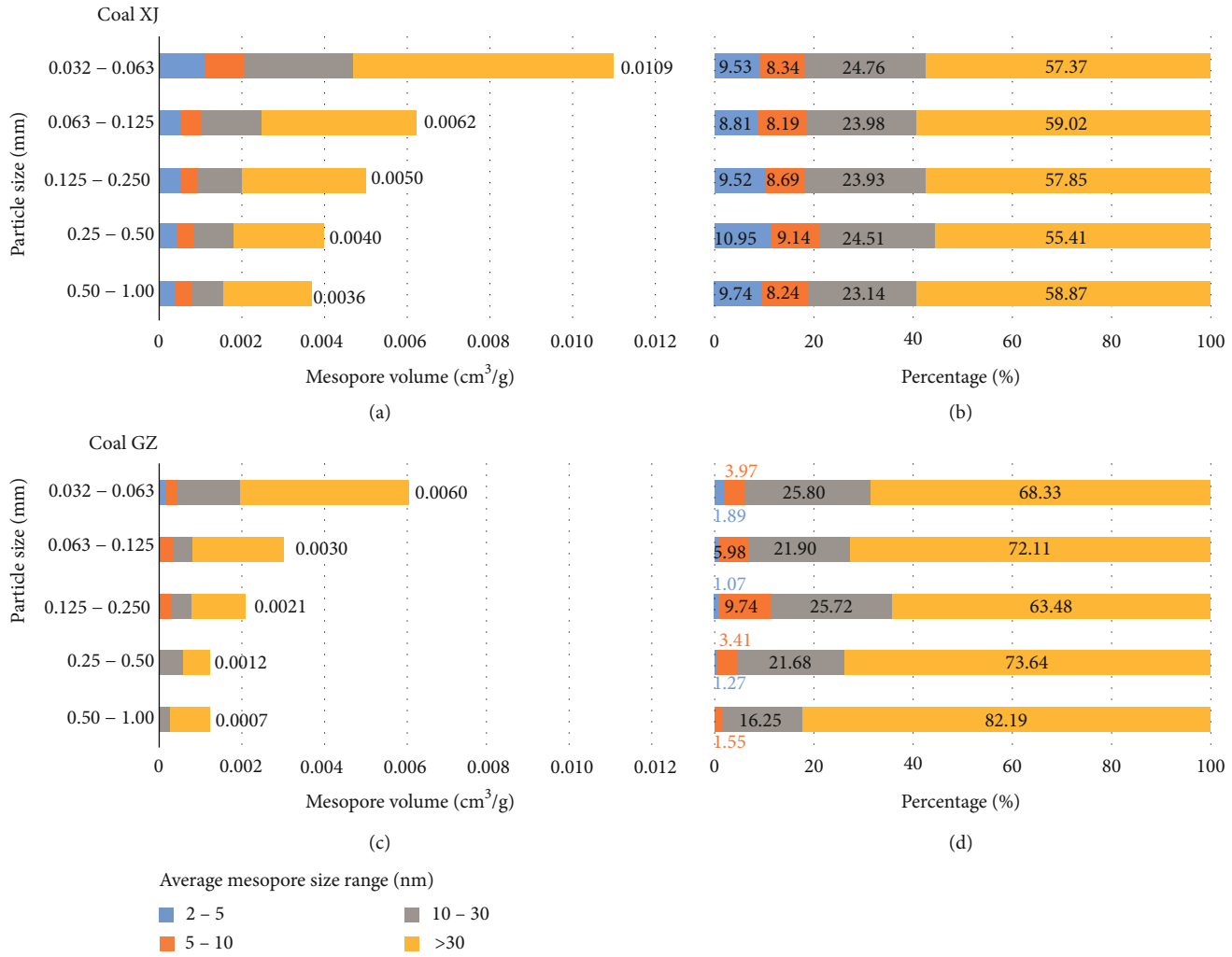

Figure 9: Horizontal and stacked bar charts of mesopore volume and proportion corresponding to specific pore size ranges for Coal XJ (a, b) and Coal GZ (c, d). Mesopore size ranges 2–5, 5–10, 10–30, and > 30 nm.

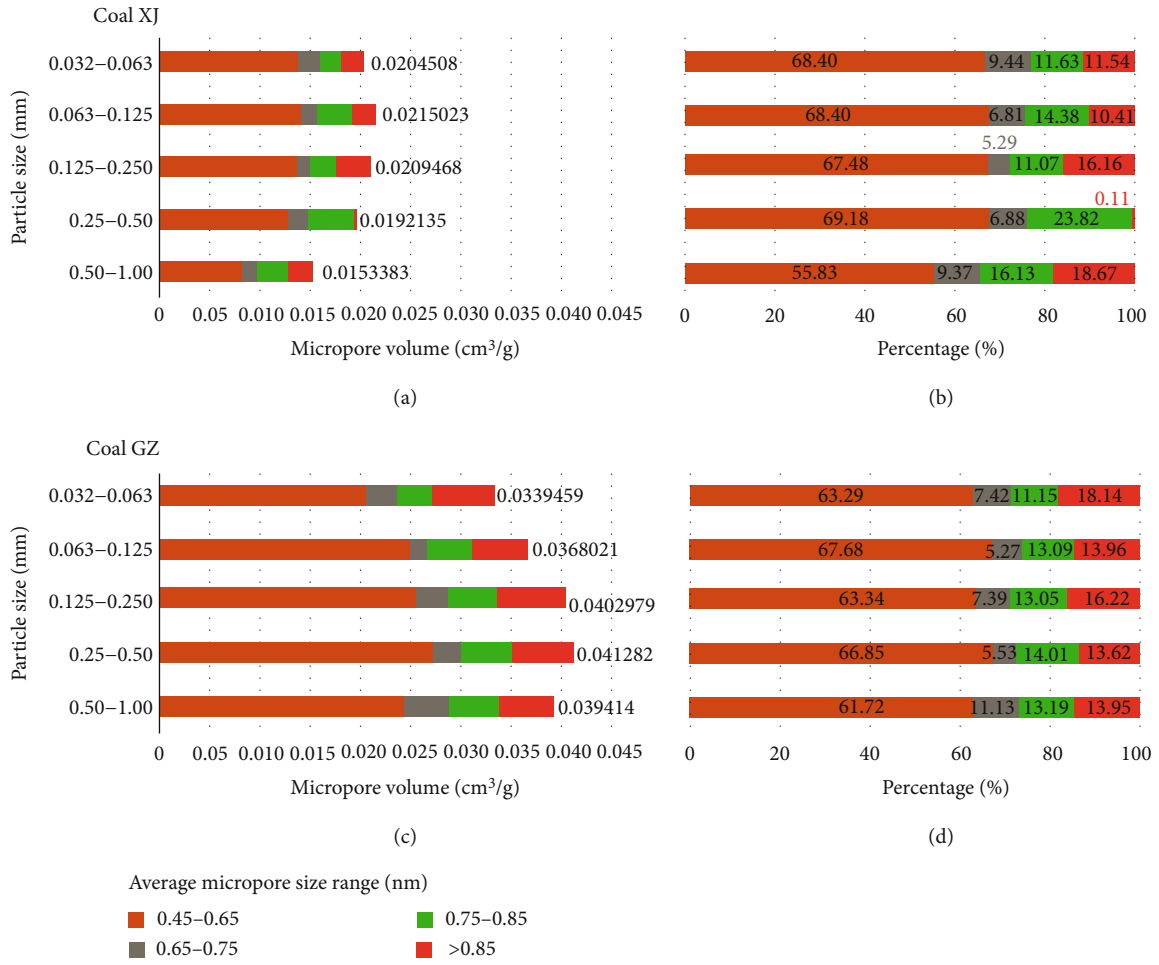

Figure 10: Horizontal and stacked bar charts of micropore volume and proportion corresponding to specific pore size ranges for Coal XJ (a, b) and Coal GZ (c, d). Micropore size ranges 0.45–0.65, 0.65–0.75, 0.75–0.85, and > 0.85 nm.

decreases from 73.00% to 44.49%, while inertinite increases from 27.00% to 55.51% with decreasing particle size. No liptinite is present in Coal XJ and Coal GZ.

3.2. Mesopore Characteristics from N_2 Adsorption Analysis. Low-pressure N_2 adsorption/desorption isotherms of Coal XJ and Coal GZ with five particle size fractions are illustrated in Figures 3(a)–3(j), respectively. The isotherms demonstrate obvious hysteresis loops caused by capillary condensation in mesopores, which are classified as type IV(a) isotherm according to the classification of physisorption [39]. The adsorption branch does not coincide with the desorption branch at low relative pressure of XJ-01 (Figure 3(a)), GZ-01 (Figure 3(f)), and GZ-02 (Figure 3(g)), which is known as low-pressure hysteresis (LPH) [38]. The LPH is mainly attributed to coal swelling, incomplete equilibrium, and the presence of N_2 that cannot be released during desorption.

Mesopore SSA and volume are listed in Table 2. Mesopore structure parameters increase with decreasing particle size (Figure 4). Mesopore SSA increases from 1.10 m^2/g to 3.12 m^2/g, and mesopore volume increases from 0.0007 cm^3/g to 0.0060 cm^3/g of Coal XJ. For Coal GZ, mesopore SSA and volume increase from 0.20 m^2/g to 1.24 m^2/g and from 0.0040 cm^3/g to 0.0109 cm^3/g, respectively. The mesopore SSA and volume of Coal XJ are higher than these of Coal GZ under the same particle size. This difference can be attributed to the coal bulk compaction resulted from coal metamorphism [13].

Mesopore PSDs of Coal XJ and Coal GZ are calculated from adsorption branches by using BJH model. As shown in Figure 5(a), mesopore PSDs of Coal XJ show similar unimodal distributions with a primary peak around 2 nm, whereas mesopore PSDs of Coal GZ are not uniform (Figure 5(b)). Mesopore PSD of GZ-04 with particle size of 0.063–0.125 mm displays a unimodal distribution with the main peak at approximately 10 nm, while mesopore PSDs of other particle size fractions exhibit bimodal distributions with the main peaks within 2–10 nm and 10–15 nm, respectively (Figure 5(b)).

3.3. Micropore Characteristics from CO_2 Adsorption Analysis. CO_2 adsorption isotherms of Coal XJ and Coal GZ with five particle size fractions are shown in Figure 6 and belong to type I(a), which are characteristics of microporous materials [39].

Using the D-A equation and the DFT method, micropore SSA and volume of Coal XJ and Coal GZ are calculated and listed in Table 2. Micropore SSA and volume of Coal XJ have small changes varying between 117.1-127.5 m^2/g and

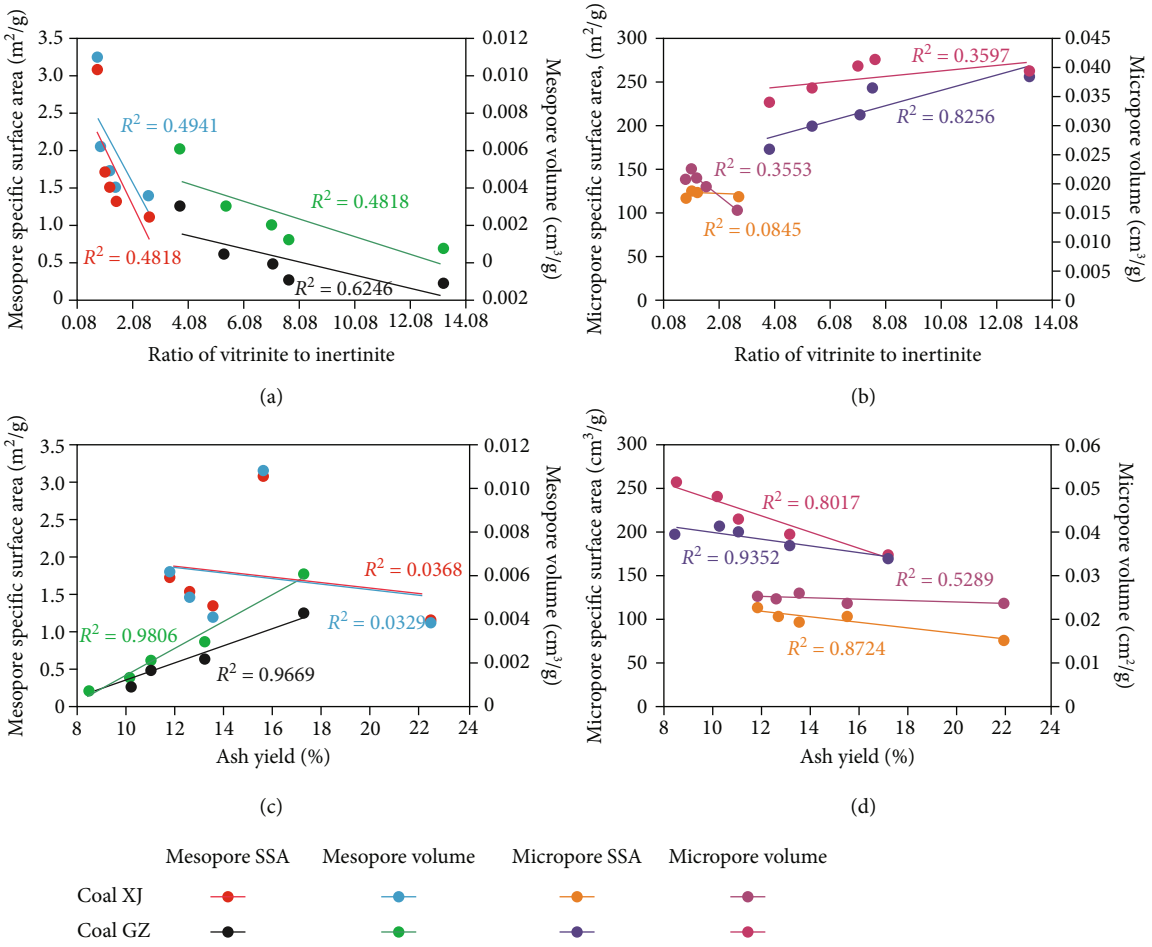

FIGURE 11: Scatter plots and linear regressions of the ratio of vitrinite to inertinite (a, b) and ash yield (c, d) versus mesopore characteristics and micropore characteristics of Coal XJ and Coal GZ.

0.0153-0.0192 cm^3/g, respectively. However, micropore SSA of Coal GZ decreases significantly from 257.3 m^2/g to 172.7 m^2/g, and micropore volume decreases from 0.0412 cm^3/g to 0.0339 cm^3/g with decreasing particle size (Figure 7). Micropore SSA and volume of Coal XJ are lower than these of Coal GZ under the same particle size. This is explained by the raising aromaticity of coal molecular structure [40–42] and a number of aromatic layers in stacking structures that provides more space for micropore formation with increasing coal rank [43].

Micropore PSD analyzed by the DFT model is illustrated in Figure 8. Micropore PSD ranges from 0.4 nm to 1.0 nm and shows the multipeak features. There are 8–12 peaks, including 3–6 major peaks in the pore size of 0.5–0.6 nm and 0.8–0.9 nm. Compared with Coal XJ, Coal GZ with the same particle size exhibits much more micropores, especially micropores at the pore size of 0.5–0.6 nm.

4. Discussion

4.1. Effect of Particle Size on Mesopore Structure Characteristics. With decreasing particle size, mesopore structure parameters increase (Figure 4). The variations are mainly attributed to the opening of the closed mesopores, which increase the accessible mesopores [33] and improve the pore accessibility to N_2 molecules during crushing [44], leading to the increasing mesopore structure parameters during the pulverization process.

Mesopore volumes and their relative proportions at different pore size ranges of Coal XJ and Coal GZ are calculated and illustrated in Figure 9. Despite mesopore volumes increase with decreasing particle size (Figures 9(a) and 9(c)), the proportions of mesopore volumes at different pore size ranges show different trends for Coal XJ and Coal GZ in the crushing process. The proportions of mesopore volumes at different pore size ranges almost remain consistent in Coal XJ (Figure 9(b)), but vary considerably in Coal GZ (Figure 9(d)). This result is consistent with the mesopore PSD characteristics with decreasing particle size (Figure 5). Chen et al. [33] thought that the increment in mesopores represents the closed mesopores that can be opened during the pulverization process. Therefore, the different variations in proportions of mesopores with decreasing particle sizes are likely to the opening of the closed mesopores. The closed mesopores with different pore sizes are opened following a certain ratio in Coal XJ, but opened irregularly in Coal GZ during the pulverization process.

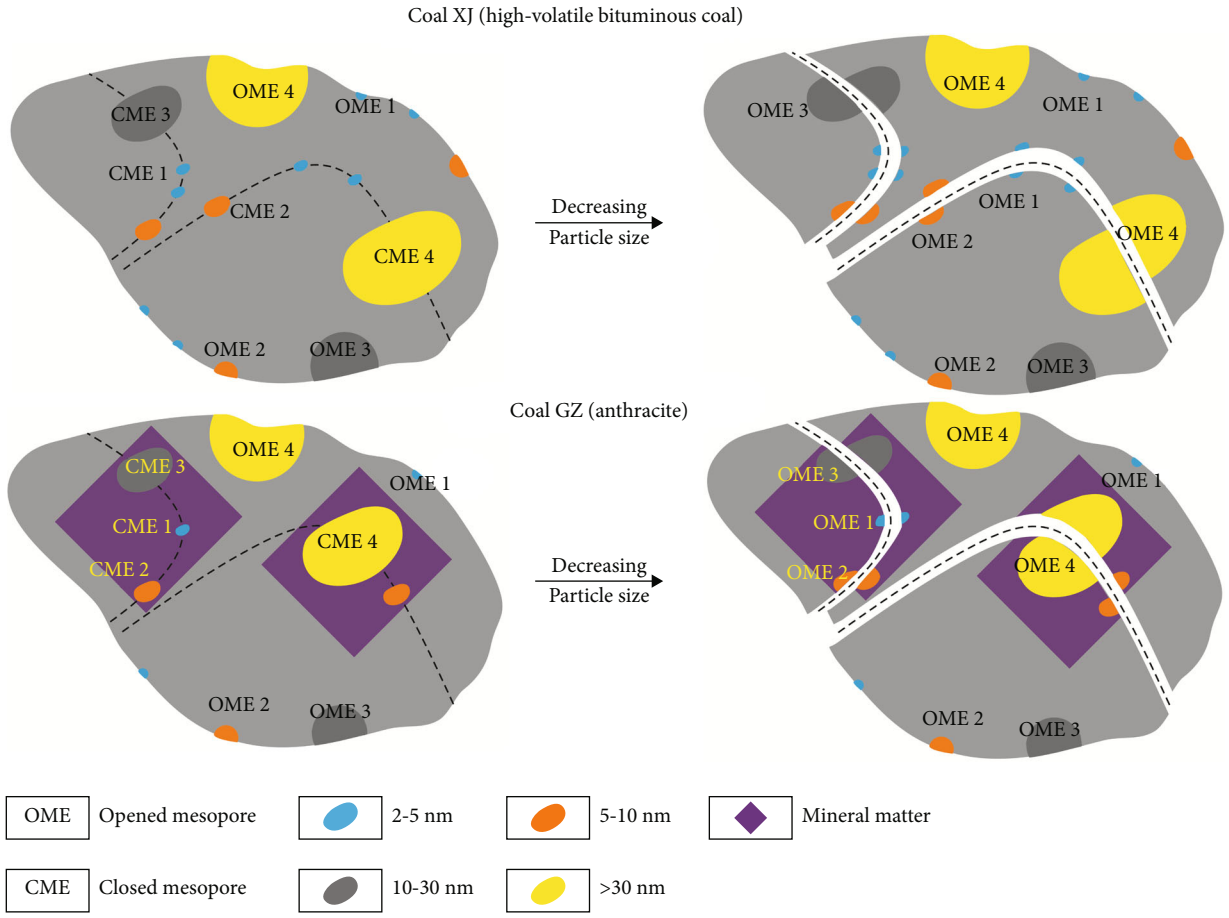

Figure 12: Evolution model of mesopore structure during the crushing process of Coal XJ and Coal GZ.

4.2. Effect of Particle Size on Micropore Structure Characteristics. The two different rank coals show different trends in micropore SSA and volume with decreasing particle size (Figure 7). Micropores are considered to be mainly related to the coal molecular structure [45–47], which remain unchanged during the crushing process. The inconsistent variations between micropore volume and SSA with decreasing particle size in the two different rank coals are observed. It is concluded that the change of micropore volume cannot be attributed to the reconstituted micropore structure with decreasing particle size.

Micropore volumes and their proportions in different pore size ranges of Coal XJ and Coal GZ are calculated and illustrated in Figure 10. Micropore volume demonstrates an increasing trend in Coal XJ and a decreasing trend in Coal GZ during crushing (Figures 10(a) and 10(c)). Particle size affects the micropore structure differently in Coal XJ and Coal GZ. The proportions of micropore volumes in different pore size ranges remain almost unchanged with decreasing particle size in Coal GZ (Figure 10(d)), but show the certain change until particle size lower than 0.25 mm in Coal XJ (Figure 10(b)). The variations in micropore volumes and their proportions in different pore size ranges with decreasing particle size need further investigation.

4.3. Effect of Fractionation on Pore Structure Characteristics. Fractionation refers to the differential accumulation of coal components including mineral matter and maceral component with crushing and sieving. Fractionation has an effect on pore structure [15, 32, 35]. In this study, mineral matter is represented by ash yield, while maceral component is analyzed using the ratio of vitrinite to inertinite (V/I).

The relationships between V/I and pore structure are plotted in Figures 11(a) and 11(b). The goodness-of-fits of V/I and mesopore structure parameters for Coal XJ and Coal GZ are lower than 0.65, which indicate the weak correlations between V/I and mesopore characteristics. The low goodness-of-fits (generally lower than 0.4) between V/I and micropore structure parameters of Coal XJ and Coal GZ imply the very weak correlations between V/I and micropore characteristics.

The relationships between ash yield and pore structure are shown in Figures 11(c) and 11(d). There are different correlations between mesopore structure parameters and ash yield in Coal XJ and Coal GZ. For Coal GZ, mesopore structure parameters and ash yield show the significant positive correlations (goodness-of-fits higher than 0.9), suggesting that mineral matter is a key factor affecting mesopore characteristics. Mineral matter contributes more mesopores than organic matter [15]. The goodness-of-fits of mesopore structure parameters and ash yield are lower than 0.1 in Coal

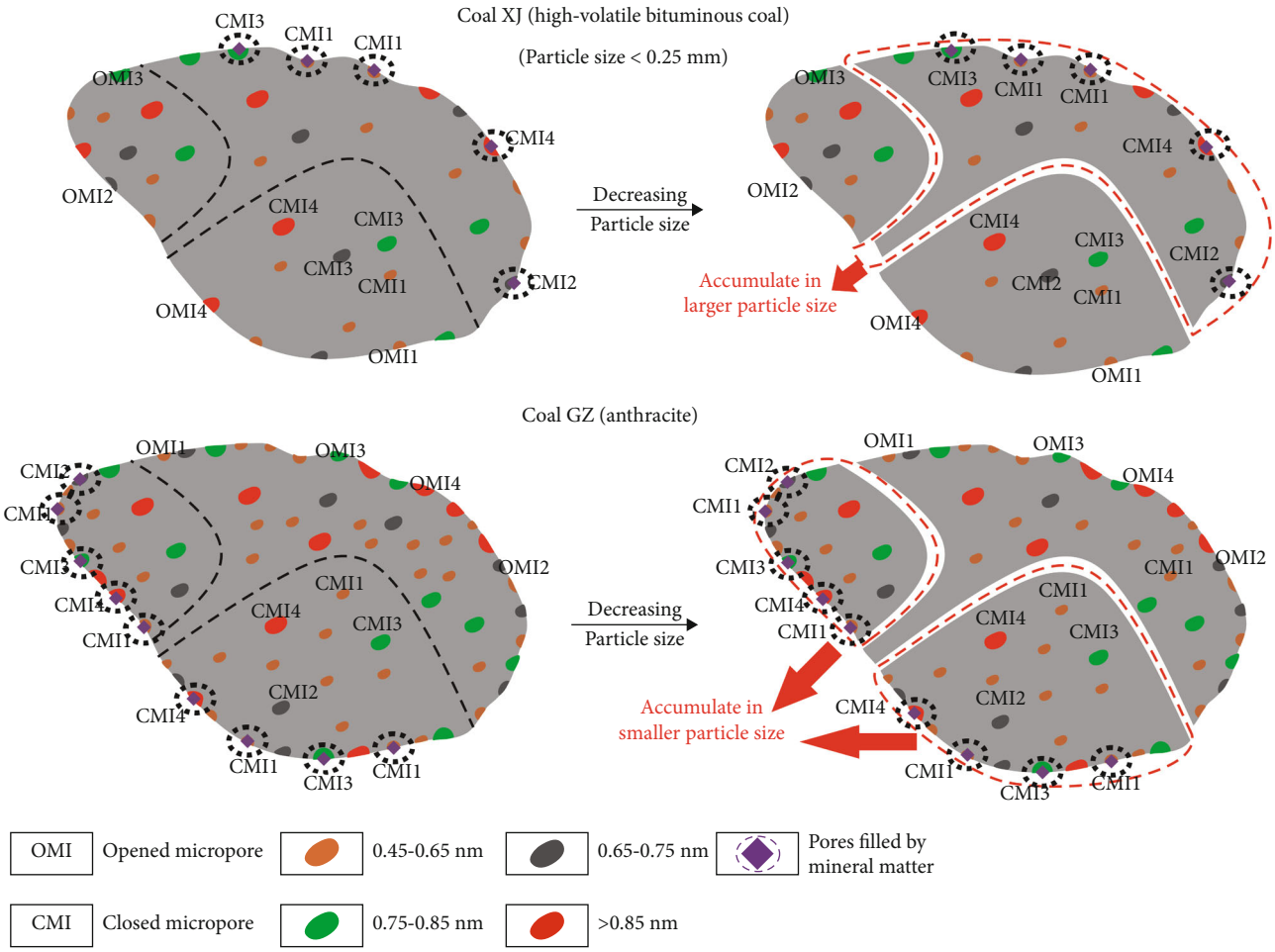

Figure 13: Evolution model of micropore structure during the crushing process of Coal XJ and Coal GZ.

XJ, which demonstrate that there is no correlation between mineral matter and mesopore characteristics. There are obvious negative correlations between micropore structure parameters and ash yield (goodness-of-fits generally lower than 0.8) in Coal XJ and Coal GZ, which are mainly due to the filling effect of mineral matter in micropores and the blocking of pore network [48], resulting in micropores becoming inaccessible to CO_2 molecules [49].

4.4. The Evolution Model of Pore Structure during Crushing Process. Based on the effects of particle size and fractionation on pore structure, the evolution models in mesopore and micropore characteristics of Coal XJ and Coal GZ during the crushing process are established, as illustrated in Figures 12 and 13, respectively.

The change in mesopore characteristics with decreasing particle size in Coal XJ and Coal GZ is strongly affected by the opening of closed mesopores during the pulverization process. Further, more mesopores including the closed mesopores exist in mineral matter in Coal GZ. The change in mesopore characteristics with decreasing particle size in Coal GZ is more heterogeneous than that in Coal XJ (Figures 9(b) and 9(c). This difference depends on that whether mineral matter affects mesopores. The closed mesopores related to mineral matter are opened irregularly, which make that the proportion of opened mesopores at different pore size ranges varies with decreasing particle size in Coal GZ. In contrast, the closed mesopores are independent of mineral matter in Coal XJ, which result in that the closed mesopores at different pore size ranges are opened following a certain ratio during the pulverization process (Figure 12).

The change in micropore characteristics with decreasing particle size in Coal XJ and Coal GZ is closely associated with the filling effect of mineral matter in micropores. Some micropores are blocked and inaccessible to CO_2 molecules, which reduce micropore volumes. Mineral matter accumulates in Coal GZ, which leads to the reduction in micropore volume (Figure 10(a)). On the contrary, mineral matter is low in Coal XJ (Table 1), and micropore volume slightly increases during crushing process (Figure 10(c)). However, the proportions of micropore volumes at different pore size ranges of Coal GZ remain unchanged during the pulverization process, indicating that the filling effect of mineral matter in micropores is unaffected by particle size. The same phenomenon is also found in Coal XJ when particle size is less than 0.25 mm (Figure 13).

4.5. The Uncertainty or Limitation of This Study. Mineral matter is replaced by ash yield to analyze the effect of mineral matter on pore characteristics in the study, which is consistent with the previous researches [15, 32, 35]. The different mediating roles of mineral matter in the two different rank coals have been preliminarily confirmed. However, mineral analysis is not conducted in this study. Subsequent mineral analysis helps to understand the effects of different mineral compositions on mesopore characteristics and micropore characteristics. For example, which mineral compositions are rich in mesopores and/or which mineral compositions can block micropores.

4.6. The Potential Application of This Study. For low-pressure N_2 adsorption, adsorption equilibrium is the primary index to select the optimal particle size [24]. For high-volatile bituminous coal, the 0.25-0.50 mm fraction and smaller fractions reach adsorption equilibrium. For anthracite, 0.125-0.250 mm fraction and smaller fractions reach adsorption equilibrium. The closed mesopores are significantly important for CBM recovery, which can be calculated from the difference in mesopores between the coarse-grained and fine-grained fractions [33]. For both high-volatile bituminous coal and anthracite, the 0.032-0.063 mm fraction contains more mesopores than other coarser fractions. Therefore, we propose 0.032-0.063 mm fraction to be the preferred particle size for low-pressure N_2 adsorption analysis.

Compared with low-pressure N_2 adsorption, low-pressure CO_2 adsorption can easily reach adsorption equilibrium, which makes that analytical particle size shows little effects on micropore characteristics [24, 32]. This is attributed to the better penetration of the multisize pore structure of coal by CO_2 molecules under the combined influence of activated diffusion, pore shrinkage, and coal swelling [14, 30, 31]. Therefore, particle size less than 1.0 mm is recommended as the optimal particle size for low-pressure CO_2 adsorption analysis.

5. Conclusions

The effect of particle size on pore structure of high-volatile bituminous coal (Coal XJ) and anthracite (Coal GZ) is investigated, and the evolution model of pore structure during the crushing process is established. The main conclusions are summarized as follows:

(1) Mesopore structure parameters are improved during the pulverization process because of the opening of the closed mesopores. The closed mesopores at different pore size ranges are opened irregularly in Coal GZ, but opened following a certain ratio in Coal XJ during pulverization

(2) The effect of particle size on micropore structure differs between Coal XJ and Coal GZ. The inconsistent trends between micropore volume and SSA with decreasing particle size suggest that the effect of particle size on micropore structure is not the result of reconstituted micropore structure

(3) Mineral matter has more mesopores than organic matter in Coal GZ, but has no relation with mesopores in Coal XJ. Mineral matter has negative effect on micropores of Coal XJ and Coal GZ

(4) The particle sizes of 0.032-0.063 mm and less than 1.0 mm are selected as the optimum particle size of low-pressure N_2 and CO_2 adsorption experiments, respectively

Abbreviations

CBM: Coalbed methane
SSA: Specific surface area
PSD: Pore size distribution
IUPAC: International Union of Pure and Applied Chemistry
BET: Brunauer-Emmett-Teller
BJH: Barrett-Joyner-Halenda
D-A: Dubinin-Astakhov
DFT: Density functional theory
LPH: Low-pressure hysteresis.

Data Availability

The data used to support the findings of this study are included within the article.

Conflicts of Interest

The authors declare no conflict of interest.

Acknowledgments

The work was financially supported by the National Natural Science Foundation of China (grant numbers 41972184, 42262022, and 41902177) and the Jiangxi Provincial Natural Science Foundation (grant number 20212BAB214030).

References

[1] T. A. Moore, "Coalbed methane: a review," *International Journal of Coal Geology*, vol. 101, pp. 36–81, 2012.

[2] R. Pan, Y. Cheng, L. Yuan, M. Yu, and J. Dong, "Effect of bedding structural diversity of coal on permeability evolution and gas disasters control with coal mining," *Natural Hazards*, vol. 73, no. 2, pp. 531–546, 2014.

[3] Y. Cai, D. Liu, Z. Pan, Y. Yao, J. Li, and Y. Qiu, "Pore structure and its impact on CH_4 adsorption capacity and flow capability of bituminous and subbituminous coals from Northeast China," *Fuel*, vol. 103, pp. 258–268, 2013.

[4] X. Fu, Y. Qin, G. G. X. Wang, and V. Rudolph, "Evaluation of coal structure and permeability with the aid of geophysical logging technology," *Fuel*, vol. 88, no. 11, pp. 2278–2285, 2009.

[5] O. P. Mahajan, "CO_2 surface area of coals: the 25-year paradox," *Carbon*, vol. 29, no. 6, pp. 735–742, 1991.

[6] O. P. Mahajan, "Physical characterization of coal," *Powder Technology*, vol. 40, no. 1-3, pp. 1–15, 1984.

[7] S. Ma, "Selection of characteristic particle size of drilling cuttings based on adsorption-desorption properties: experiment and simulation," *Adsorption Science & Technology*, vol. 2022, article 2894099, pp. 1–19, 2022.

[8] IUPAC, "Recommendations for the characterization of porous solids (technical report)," *Pure and Applied Chemistry*, vol. 66, no. 8, pp. 1739–1758, 1994.

[9] Y. Zhao, Y. Sun, S. Liu, K. Wang, and Y. Jiang, "Pore structure characterization of coal by NMR cryoporometry," *Fuel*, vol. 190, pp. 359–369, 2017.

[10] J. Li, Q. Huang, G. Wang, and E. Wang, "Influence of active water on gas sorption and pore structure of coal," *Fuel*, vol. 310, article 122400, 2022.

[11] Z. Qu, G. G. X. Wang, B. Jiang, V. Rudolph, X. Dou, and M. Li, "Experimental study on the porous structure and compressibility of tectonized coals," *Energy & Fuels*, vol. 24, no. 5, pp. 2964–2973, 2010.

[12] C. Laxminarayana and P. J. Crosdale, "Role of coal type and rank on methane sorption characteristics of Bowen Basin, Australia coals," *International Journal of Coal Geology*, vol. 40, no. 4, pp. 309–325, 1999.

[13] B. Nie, X. Liu, L. Yang, J. Meng, and X. Li, "Pore structure characterization of different rank coals using gas adsorption and scanning electron microscopy," *Fuel*, vol. 158, pp. 908–917, 2015.

[14] J. F. Unsworth, C. S. Fowler, and L. F. Jones, "Moisture in coal: 2. Maceral effects on pore structure," *Maceral effects on pore structure. Fuel*, vol. 68, no. 1, pp. 18–26, 1989.

[15] M. Mastalerz, A. Drobniak, D. Strąpoć, W. Solano Acosta, and J. Rupp, "Variations in pore characteristics in high volatile bituminous coals: implications for coal bed gas content," *International Journal of Coal Geology*, vol. 76, no. 3, pp. 205–216, 2008.

[16] W. Han, G. Zhou, D. Gao et al., "Experimental analysis of the pore structure and fractal characteristics of different metamorphic coal based on mercury intrusion-nitrogen adsorption porosimetry," *Powder Technology*, vol. 362, pp. 386–398, 2020.

[17] J. Jiang, W. Yang, Y. Cheng, K. Zhao, and S. Zheng, "Pore structure characterization of coal particles via MIP, N_2 and CO_2 adsorption: effect of coalification on nanopores evolution," *Powder Technology*, vol. 354, pp. 136–148, 2019.

[18] Y. Li, C. Zhang, D. Tang et al., "Coal pore size distributions controlled by the coalification process: an experimental study of coals from the Junggar, Ordos and Qinshui basins in China," *Fuel*, vol. 206, pp. 352–363, 2017.

[19] F. Wang, Y. Cheng, S. Lu, K. Jin, and W. Zhao, "Influence of coalification on the pore characteristics of middle–high rank coal," *Energy & Fuels*, vol. 28, pp. 5729–5736, 2014.

[20] R. Zhang, S. Liu, J. Bahadur et al., "Estimation and modeling of coal pore accessibility using small angle neutron scattering," *Fuel*, vol. 161, pp. 323–332, 2015.

[21] O. O. Adeboye and R. M. Bustin, "Variation of gas flow properties in coal with probe gas, composition and fabric: examples from western Canadian sedimentary basin," *International Journal of Coal Geology*, vol. 108, pp. 47–52, 2013.

[22] Y. Zhao, S. Liu, D. Elsworth, Y. Jiang, and J. Zhu, "Pore structure characterization of coal by synchrotron small-angle X-ray scattering and transmission electron microscopy," *Energy & Fuels*, vol. 28, no. 6, pp. 3704–3711, 2014.

[23] Y. Li, J. Yang, Z. Pan, and W. Tong, "Nanoscale pore structure and mechanical property analysis of coal: an insight combining AFM and SEM images," *Fuel*, vol. 260, article 116352, 2020.

[24] M. Mastalerz, L. Hampton, A. Drobniak, and H. Loope, "Significance of analytical particle size in low-pressure N_2 and CO_2 adsorption of coal and shale," *International Journal of Coal Geology*, vol. 178, pp. 122–131, 2017.

[25] Z. Wang, Y. Cheng, G. Wang, G. Ni, and L. Wang, "Comparative analysis of pore structure parameters of coal by using low pressure argon and nitrogen adsorption," *Fuel*, vol. 309, article 122120, 2022.

[26] S. Zhou, D. Liu, Y. Cai, Y. Yao, Y. Che, and Z. Liu, "Multi-scale fractal characterizations of lignite, subbituminous and high-volatile bituminous coals pores by mercury intrusion porosimetry," *Journal of Natural Gas Science and Engineering*, vol. 44, pp. 338–350, 2017.

[27] Y. Zhao, Y. Sun, S. Liu, Z. Chen, and L. Yuan, "Pore structure characterization of coal by synchrotron radiation nano-CT," *Fuel*, vol. 215, pp. 102–110, 2018.

[28] G. N. Okolo, R. C. Everson, H. W. J. P. Neomagus, M. J. Roberts, and R. Sakurovs, "Comparing the porosity and surface areas of coal as measured by gas adsorption, mercury intrusion and SAXS techniques," *Fuel*, vol. 141, pp. 293–304, 2015.

[29] Z. Li, D. Liu, Y. Cai, Y. Wang, and J. Teng, "Adsorption pore structure and its fractal characteristics of coals by N_2 adsorption/desorption and FESEM image analyses," *Fuel*, vol. 257, article 116031, 2019.

[30] P. I. Ravikovitch, B. W. Bogan, and A. V. Neimark, "Nitrogen and carbon dioxide adsorption by soils," *Environmental Science & Technology*, vol. 39, no. 13, pp. 4990–4995, 2005.

[31] M. Thommes and K. A. Cychosz, "Physical adsorption characterization of nanoporous materials: progress and challenges," *Adsorption*, vol. 20, no. 2-3, pp. 233–250, 2014.

[32] S. Hou, X. Wang, X. Wang, Y. Yuan, S. Pan, and X. Wang, "Pore structure characterization of low volatile bituminous coals with different particle size and tectonic deformation using low pressure gas adsorption," *International Journal of Coal Geology*, vol. 183, pp. 1–13, 2017.

[33] Y. Chen, Y. Qin, C. Wei et al., "Porosity changes in progressively pulverized anthracite subsamples: implications for the study of closed pore distribution in coals," *Fuel*, vol. 225, pp. 612–622, 2018.

[34] L. Si, Z. Li, Y. Yang et al., "Experimental investigation for pore structure and CH4 release characteristics of coal during pulverization process," *Energy & Fuels*, vol. 31, no. 12, pp. 14357–14366, 2017.

[35] Z. Wang, Y. Cheng, Y. Qi, R. Wang, L. Wang, and J. Jiang, "Experimental study of pore structure and fractal characteristics of pulverized intact coal and tectonic coal by low temperature nitrogen adsorption," *Powder Technology*, vol. 350, pp. 15–25, 2019.

[36] S. Zhang, H. Liu, C. Wu, and Z. Jin, "Influence of particle size on pore structure and multifractal characteristics in coal using low-pressure gas adsorption," *Journal of Petroleum Science and Engineering*, vol. 212, article 110273, 2022.

[37] P. Ren, H. Xu, D. Tang et al., "Pore structure and fractal characterization of main coal-bearing synclines in western Guizhou, China," *Journal of Natural Gas Science and Engineering*, vol. 63, pp. 58–69, 2019.

[38] F. Rouquerol, J. Rouquerol, and K. Sing, *Adsorption by Powders and Porous Solids Principles, Methodology and Applications*, Academic Press, London, 2nd edition, 2014.

[39] M. Thommes, K. Kaneko, A. V. Neimark et al., "Physisorption of gases, with special reference to the evaluation of surface area and pore size distribution (IUPAC technical report)," *Pure and Applied Chemistry*, vol. 87, no. 9-10, pp. 1051–1069, 2015.

[40] J. Wollenweber, J. Schwarzbauer, R. Littke, H. Wilkes, A. Armstroff, and B. Horsfield, "Characterisation of non-extractable macromolecular organic matter in Palaeozoic coals," *Palaeogeography, Palaeoclimatology, Palaeoecology*, vol. 240, no. 1-2, pp. 275–304, 2006.

[41] R. M. Bustin and Y. Guo, "Abrupt changes (jumps) in reflectance values and chemical compositions of artificial charcoals and inertinite in coals," *International Journal of Coal Geology*, vol. 38, no. 3-4, pp. 237–260, 1999.

[42] L. Zieger, R. Littke, and J. Schwarzbauer, "Chemical and structural changes in vitrinites and megaspores from carboniferous coals during maturation," *International Journal of Coal Geology*, vol. 185, pp. 91–102, 2018.

[43] B. Feng and S. K. Bhatia, "Variation of the pore structure of coal chars during gasification," *Carbon*, vol. 41, no. 3, pp. 507–523, 2003.

[44] A. Busch, Y. Gensterblum, B. M. Krooss, and R. Littke, "Methane and carbon dioxide adsorption-diffusion experiments on coal: upscaling and modeling," *International Journal of Coal Geology*, vol. 60, no. 2-4, pp. 151–168, 2004.

[45] J.-L. Faulon, J. P. Mathews, G. A. Carlson, and P. G. Hatcher, "Correlation between microporosity and fractal dimension of bituminous coal based on computer-generated models," *Energy & Fuels*, vol. 8, no. 2, pp. 408–414, 1994.

[46] Y. Liu, Y. Zhu, W. Li, C. Zhang, and Y. Wang, "Ultra micropores in macromolecular structure of subbituminous coal vitrinite," *Fuel*, vol. 210, pp. 298–306, 2017.

[47] L. R. Radovic, V. C. Menon, C. A. L. Y. Leon et al., "On the porous structure of coals: evidence for an interconnected but constricted micropore system and implications for coalbed methane recovery," *Adsorption*, vol. 3, no. 3, pp. 221–232, 1997.

[48] P. D. Gamson, B. B. Beamish, and D. P. Johnson, "Coal microstructure and micropermeability and their effects on natural gas recovery," *Fuel*, vol. 72, no. 1, pp. 87–99, 1993.

[49] R. Sakurovs, L. He, Y. B. Melnichenko et al., "Pore size distribution and accessible pore size distribution in bituminous coals," *International Journal of Coal Geology*, vol. 100, pp. 51–64, 2012.